

# Discovery potential for $T' \rightarrow tZ$ in the trilepton channel at the LHC

---

**Lorenzo Basso<sup>a\*</sup> and Jeremy Andrea<sup>b</sup>**

*Université de Strasbourg, IPHC, 23 rue du Loess 67037 Strasbourg, France  
CNRS, UMR7178, 67037 Strasbourg, France*

<sup>a</sup>*Email:* lorenzo.basso@iphc.cnrs.fr

<sup>b</sup>*Email:* jeremy.andrea@iphc.cnrs.fr

<sup>\*</sup>*Corresponding author*

**ABSTRACT:** The LHC discovery potential of heavy top partners decaying into a top quark and a  $Z$  boson is studied in the trilepton channel at  $\sqrt{s} = 13$  TeV. The clean multilepton final state allows to strongly reduce the background contaminations and to reconstruct the  $T'$  mass. We show that a simple cut-and-count analysis probes the parameter space of a simplified model as efficiently as a dedicated multivariate analysis. The trilepton signature finally turns out to be as sensitive in the low  $T'$  mass region as the complementary channel with a fully hadronic top quark, and more sensitive in the large mass domain. The reinterpretation in terms of the top- $Z$ -up anomalous coupling is shown.

**KEYWORDS:** Top partner, trilepton, discovery potential, simplified model, MVA.

---

## Contents

<b>1. Introduction</b>	<b>1</b>
<b>2. Simplified model</b>	<b>2</b>
2.1 Cross section parameterisation	3
<b>3. Event analysis</b>	<b>4</b>
3.1 Cut-and-count	6
3.2 Multivariate analysis	7
3.3 Results	9
3.4 Top FCNC reinterpretation	11
<b>4. Conclusions</b>	<b>12</b>

---

## 1. Introduction

In 2012 the Run-I of the LHC at the center of mass energies of 7 and 8 TeV has finally discovered the long sought-after Higgs boson [1, 2]. In Spring 2015 the LHC will start again to produce  $pp$  collisions in the so-called Run-II, at the increased energy of 13 TeV. It is expected to accumulate  $100 - 150$  inverse femtobarn ( $\text{fb}^{-1}$ ) of data in the first two years and up to  $300 \text{ fb}^{-1}$  in the following ones. The primary scope of the Run-II is to further understand the newly discovered Higgs boson and to eventually make new discoveries. In all generality, it is very common in beyond the standard model theories that new heavy fermions arise to stabilise the Higgs boson mass and to protect it from dangerous quadratic divergences. In many cases, these new fermions are heavy partners of the third generation quarks with vector-like couplings. They are commonly predicted by many new physics scenarios, including Extra Dimensions, Little Higgs Models, and Composite Higgs Models [3, 4, 5, 6, 7, 8, 9]. The observation of new heavy quarks thus plays an important role in the investigation of the Higgs sector. The common feature of these heavy quarks is to decay into a standard model quark and a  $W^\pm$  boson, a  $Z$  bosons, or a Higgs boson<sup>1</sup>. The relative branching ratios are purely determined by the weak quantum numbers of the multiplet the new quark belongs to [10]. Here we will focus on the case of a singlet heavy quark: the *top partner* or  $T'$ . Experimental collaborations are now considering the interplay between the various decay channels in their searches. Recent limits from ATLAS [11] and CMS [12] lie within 690-780 GeV, depending on the considered final state.

These searches however do not typically consider intergenerational mixing. Although vector-like quarks are usually assumed to only mix with the third generation following

---

<sup>1</sup>Other possibilities like 3-body decays are also possible, but are not covered here.

hierarchy or naturalness arguments [13, 14, 15, 16], the top partners can mix in a sizable way with lighter quarks while remaining compatible with the current experimental constraints [17, 18]. This possibility has been recently pursued and must be considered with attention. The top partners interactions with the electroweak and Higgs bosons are generically allowed through arbitrary Yukawa couplings, implying that the branching ratios into light quarks can be possibly competitive with the top-quark one.

Beside opening up the decay channel into a standard model boson plus a light quark, the mixing with lighter generations also enhances the single production, especially due to the presence of first generation valence quarks in the initial state. Even without mixing, the single production cross sections at the upcoming LHC energies become competitive with the pair production ones. Furthermore, the  $T' \rightarrow tZ$  final state is only recently being experimentally investigated, both in the dilepton and in the trilepton channels by ATLAS [11]. Following the investigation first pursued at the 2013 Les Houches workshop [19], in this paper we study the LHC discovery potential of the  $T' \rightarrow tZ$  channel in the trilepton decay mode in single production at  $\sqrt{s} = 13$  TeV. To capture all the essential features of the new heavy top quark while remaining as model independent as possible, the study here presented is performed in the framework of simplified models. We will employ the dedicated model for the heavy singlet top partner as presented in Ref. [18], comprising only 3 independent couplings.

The paper is structured as follows. In section 2 the simplified model under consideration is described. In addition, we propose a convenient way to explore its parameter space. In section 3 we describe our analysis, comparing the discovery reach obtained in a simple cut-and-count approach to that obtained in a dedicated multivariate analysis. Results for  $\mathcal{L} = 100 \text{ fb}^{-1}$  are collected in section 3.3. The main result of this paper is that the simple cut-and-count analysis probes the  $T'$  parameter space as efficiently as the more sophisticated multivariate analysis. Also, a comparison to the complementary dilepton channel, recently presented in [20] for a  $T'$  coupling only to the third generation, is pursued. The reinterpretation of our results to the case of the top-quark flavour-changing neutral coupling to an up-quark and a  $Z$  boson is overviewed in section 3.4. Finally, we conclude in section 4.

## 2. Simplified model

A simple Lagrangian that parametrises the  $T'$  couplings to quarks and electroweak boson is (showing only the couplings relevant for our analysis) [18]

$$\mathcal{L}_{T'} = g^* \left\{ \sqrt{\frac{R_L}{1+R_L}} \frac{g}{\sqrt{2}} [\overline{T'}_L W_\mu^+ \gamma^\mu d_L] + \sqrt{\frac{1}{1+R_L}} \frac{g}{\sqrt{2}} [\overline{T'}_L W_\mu^+ \gamma^\mu b_L] + \right. \\ \left. \sqrt{\frac{R_L}{1+R_L}} \frac{g}{2 \cos \theta_W} [\overline{T'}_L Z_\mu \gamma^\mu u_L] + \sqrt{\frac{1}{1+R_L}} \frac{g}{2 \cos \theta_W} [\overline{T'}_L Z_\mu \gamma^\mu t_L] \right\} + h.c. , \quad (2.1)$$

where the subscripts  $L$  and  $R$  label the chiralities of the fermions. Only 3 parameters are sufficient to fully describe the interactions that are relevant for our investigation. Besides  $M_{T'}$ , the vector-like mass of the top partner, there are the 2 couplings appearing in eq. (2.1)

- $g^*$ , the coupling strength to SM quarks in units of standard couplings, which is only relevant in single production. The cross sections for the latter scale with the coupling squared;
- $R_L$ , the generation mixing coupling, which describes the rate of decays to first generation quarks with respect to the third generation, so that  $R_L = 0$  corresponds to coupling to top and bottom quarks only, while the limit  $R_L = \infty$  represent coupling to light quarks only.

For some possible reinterpretation of this effective Lagrangian in terms of complete models, see Refs. [9, 20].

## 2.1 Cross section parameterisation

The  $pp \rightarrow T'j \rightarrow tZj$  process studied here is given by the set of Feynman diagrams displayed in Fig.1.

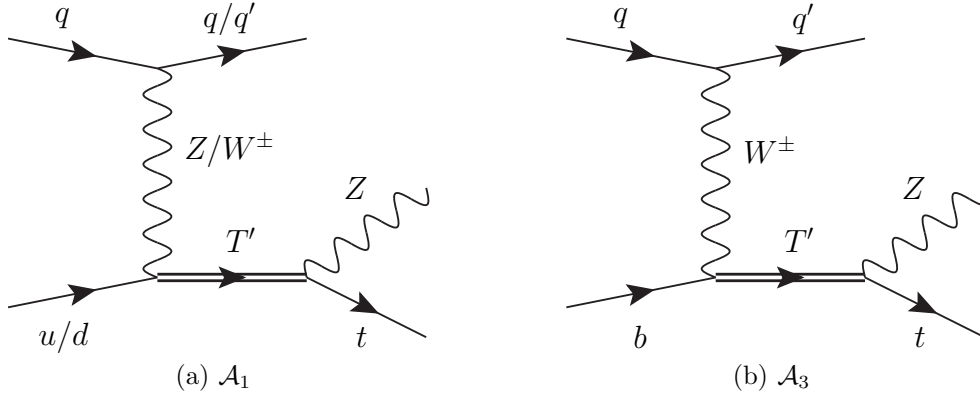


Figure 1: Feynman diagrams for the process  $pp \rightarrow T'j \rightarrow tZj$  via couplings of the  $T'$  to (a) first generation quarks and (b) third generation quarks.

There are two sets of diagrams, i.e. where the  $T'$  is produced due to the interaction with light quarks ( $\mathcal{A}_1$ ) or due to the interaction with the  $b$  quark ( $\mathcal{A}_3$ ). From the Lagrangian in eq. (2.1), these 2 sets of diagrams give production cross sections that scale differently with  $R_L$ , the mixing coupling. Further, the decay into a top quark and a  $Z$  boson scales with  $R_L$  too. We parametrise the production cross section and branching ratio  $\text{BR}(T' \rightarrow tZ)$  as follows:

$$\sigma_{pp \rightarrow T'}(M_{T'}, R_L) = \mathcal{A}_1(M_{T'}) \frac{R_L}{1 + R_L} + \mathcal{A}_3(M_{T'}) \frac{1}{1 + R_L}, \quad (2.2)$$

$$\text{BR}_{T' \rightarrow tZ}(M_{T'}, R_L) = \mathcal{B}(M_{T'}) \frac{1}{1 + R_L}, \quad (2.3)$$

where  $\mathcal{A}_i(M_{T'})$  ( $i = 1, 3$ ) and  $\mathcal{B}(M_{T'})$  are numerical coefficients. In details,  $\mathcal{A}_i$  represents the production cross section for the heavy quark due to interactions to partons belonging to the  $i^{\text{th}}$  generation, while  $\mathcal{B}$  is the  $T'$  branching ratio for its decay into a top quark and a

Z boson<sup>2</sup>. They have been evaluated at the LHC at  $\sqrt{s} = 13$  TeV for the CTEQ6L PDF [21] and collected in table 1.

$M_{T'}$ (GeV)	$\mathcal{A}_1(M_{T'})$ (pb)	$\mathcal{A}_3(M_{T'})$ (pb)	$\mathcal{B}(M_{T'})$ (%)
800	1.2614	0.07242	22.4
1000	0.7752	0.03518	23.5
1200	0.5001	0.01826	24.0
1400	0.3331	0.00994	24.2
1600	0.2265	0.00561	24.4

Table 1: Numerical coefficients for cross sections and branching ratios.

These formulas will allow us to draw the LHC discovery power curves as a function of  $R_L$  in section 3.3 in a simple way. The product of eq. (2.2) and eq. (2.3) gives the cross section for  $pp \rightarrow T'j \rightarrow tZj$  as a function of  $R_L$  in the narrow-width approximation. However, this also depends on the choice of the PDF, on the top mass, the EW couplings, etc. By considering the ratio of the cross sections evaluated at different values of  $R_L$  (and all other input fixed) one can factorise the impact of the former. Such ratio can then be used to rescale a given cross section, evaluated at the user's choice of the input parameters, as a function of  $R_L$ . In our case, we computed the cross section of the various benchmark points for  $R_L = 0.5$ , hence their cross section for an arbitrary value of  $R_L$  is given by

$$\sigma(M_{T'}, R_L) = \sigma(M_{T'}, 0.5) \frac{\sigma_{pp \rightarrow T'}(M_{T'}, R_L) BR_{T' \rightarrow tZ}(M_{T'}, R_L)}{\sigma_{pp \rightarrow T'}(M_{T'}, 0.5) BR_{T' \rightarrow tZ}(M_{T'}, 0.5)}. \quad (2.4)$$

Furthermore, this rescaling can be applied anywhere in the cutflow, i.e., after any cut.

### 3. Event analysis

All samples employed in this study have been generated in **MadGraph5\_aMC@NLO v2.1.2** [22] with the **CTEQ6L1** PDF [21]. Events have subsequently been hadronised/parton showered in **PYTHIA 6** [23] with tune **Z2** [24]. Detector simulation is performed with a customised version of **Delphes 3** [25] to emulate the CMS detector. Jets have been reconstructed with **FastJet** [26] employing the anti- $k_t$  algorithm [27] with parameter  $R = 0.5$ .

The signal (S) is generated at leading order from the model implemented in **FeynRules** [28, 29]. We generate 5 benchmark points varying the  $T'$  mass in steps of 200 GeV in the range

$$M_{T'} \in [800; 1600] \text{ GeV}, \quad (3.1)$$

with  $g^* = 0.1$  and  $R_L = 0.5$ . We do not apply here any  $k$ -factor to the signal.

Backgrounds (B) that can give 3 leptons in the final state which are considered in this analysis are:  $t\bar{t}$  and  $Z/W + jets$  with non-prompt leptons, and  $t\bar{t}W$ ,  $t\bar{t}Z$ ,  $tZj$  and  $WZ$  with only genuinely prompt leptons. We generated leading order samples with up to 2 merged

---

<sup>2</sup>Eq. (2.3) holds when all the  $T'$  decay products are much lighter than its mass, which is the case under consideration.

jets normalised to the (N)NLO cross section where available, taken from [22, 30]. For both signal and background, a suitable number of unweighted event is generated. We checked that the statistical uncertainties at any point of our analyses are below 1%, and for this reason they will not be quoted.

We do not simulate multijet backgrounds, which can be reliably estimated only from data. Further, we do not consider jets faking electrons, since this is a feature which is not supported in **Delphes**. It is however seen to be negligible in multileptons analyses (see for instance, Ref. [31]).

The analysis is carried out in **MadAnalysis 5** [32, 33]. Leptons ( $\ell = e, \mu$ ) and jets are identified if passing the following criteria:

$$p_T(\ell) > 20\text{GeV}, \quad |\eta(e/\mu)| < 2.5/2.4, \quad (3.2)$$

$$p_T(j) > 40\text{GeV}, \quad |\eta(j)| < 5, \quad (3.3)$$

$$\Delta R(\ell, j) > 0.4 \quad (3.4)$$

External routines for  $b$ -tagging and for lepton isolation have been implemented. Regarding the former, here we adopted the medium working point [34], which has an average  $b$ -tagging rate of 70% and a light mistag rate of 1%. To apply the  $b$ -tagging, we considered jets within the tracker only, i.e. with  $|\eta(j)| < 2.4$ . This means that the  $b$ -tagging probability for jets with larger pseudorapidities is vanishing. For the latter, the combined tracker-calorimetric isolation is used, with a cone radius of 0.3 and  $I_{rel} = 0.10$ . This choice has been taken as a compromise to strongly reduce backgrounds with non-prompt leptons without suppressing the signal, where the two leptons coming from the  $Z$  boson get closer and closer as the top partner mass increases.

After the object reconstruction and selection, we apply some general preselections as follows: we require at least 1 jet and no more than 3, of which exactly one is  $b$ -tagged, and exactly 3 leptons (electrons or muons). The requirement of less than 3 jets removes the  $T'$  pair production isolating the single production channel.

Efficiencies and event yields are evaluated for  $\mathcal{L} = 100 \text{ fb}^{-1}$  and are collected in table 2. The requirement of 3 isolated leptons strongly reduces the  $t\bar{t} + X$  backgrounds, especially the  $t\bar{t} + jets$  one. The diboson component is instead suppressed by the  $b$ -tagging. Regarding the signal, the requirement of 3 isolated leptons is less efficient as the  $T'$  mass increases. This is because the 2 leptons stemming from the  $Z$  boson gets closer to each other as the  $T'$  gets heavier, due to the larger boost of the  $Z$  boson in the  $T' \rightarrow t Z$  decay.

Finally, the pair of same-flavour and opposite-sign leptons closest to the  $Z$  boson mass is chosen, and a cut around their invariant mass distribution is performed,

$$|M(\ell^+ \ell^-) - M_Z| < 15 \text{ GeV}. \quad (3.5)$$

The lepton from the top decay is therefore identified as the remaining one in our trilepton channel and labelled  $\ell_W$ .

We describe in the following the 2 analyses we performed, that differentiate from this point on. The first one is a traditional cut-and-count strategy, where subsequent cuts are applied to the most important kinematic variables to maximise the signal-over-background

Background	no cuts	$1 \leq n_j \leq 3$	$n_\ell \equiv 3$	$n_b \equiv 1$
$t\bar{t}(+X)$	$7.5 \cdot 10^6$ (100%)	$6.1 \cdot 10^6$ (81.2%)	514.9 (0.09%)	243.8 (47.3%)
$tZj$	3521 (100%)	2953 (83.9%)	290.6 (9.8%)	170.0 (58.5%)
$WZ$	$1.4 \cdot 10^5$ (100%)	$5.7 \cdot 10^4$ (41.9%)	3883 (6.9%)	164.3 (4.2%)
Total	$7.6 \cdot 10^6$ (100%)	$6.1 \cdot 10^6$ (80.5%)	4689 (0.08%)	578.0 (12.3%)
$M_{T'}$ (GeV)	no cuts	$1 \leq n_j \leq 3$	$n_\ell \equiv 3$	$n_b \equiv 1$
800	119.7 (100%)	105.0 (87.8%)	39.3 (37.4%)	25.5 (64.8%)
1000	77.1 (100%)	67.8 (87.9%)	26.0 (38.4%)	16.4 (63.2%)
1200	52.0 (100%)	45.3 (87.2%)	16.1 (35.6%)	10.1 (62.4%)
1400	35.3 (100%)	30.5 (86.6%)	8.0 (26.1%)	4.8 (60.1%)
1600	24.5 (100%)	21.1 (86.0%)	3.8 (18.0%)	2.2 (58.3%)

Table 2: Events surviving the preselections and relative efficiencies (with respect to the previous item). Signal computed for  $g^* = 0.1$  and  $R_L = 0.5$ .

ratio. The second one is a multivariate analysis (MVA), where several discriminating observables are used at once to distinguish the signal from the background, cutting at the end only on its output.

### 3.1 Cut-and-count

The first strategy to study the LHC discovery potential illustrated here is the cut-and-count one (C&C). As for the previous reconstruction of the  $Z$  boson from its decay products, one could also reconstruct both the top quark and the  $W$  boson stemming from its decay. The presence of only one source of missing energy (one neutrino) allows to reconstruct the four momentum of the latter by imposing suitable kinematical constraints. Hence one can reconstruct the  $W$  boson and the top quark as resonances in the invariant mass as well as in the transverse mass distributions of the decay products. We chose to use the latter, in the following formulation [35]:

$$m_T^2 = \left( \sqrt{M^2(vis) + P_T^2(vis) + |\vec{p}_T|^2} \right)^2 - \left( \vec{P}_T(vis) + \vec{\vec{p}}_T \right)^2, \quad (3.6)$$

because of the sharper peaks as compared to those in the invariant mass distributions. Instead to draw suitable window mass cuts, we decided to only apply loose selections, which maximise their efficiencies while retaining most of the signal. The cuts we applied are as follows:

$$10 < M_T(\ell_W)/\text{GeV} < 150, \quad (3.7)$$

$$0 < M_T(\ell_W b)/\text{GeV} < 220. \quad (3.8)$$

In particular, the lower cut in eq. (3.7) is inspired by experimental analyses to suppress the multijet background, which we did not simulate.

Surviving events and relative efficiencies are collected in table 3. The numerical values of the cuts appearing in eqs. (3.5)–(3.8) have been chosen to maximise the signal-over-background ratio while keeping at least 90% of the signal.

Background	$n_b \equiv 1$	cut (3.5)	cut (3.7)	cut (3.8)
$t\bar{t}(+X)$	243.8 (47.3%)	154.8 (63.5%)	135.1 (87.3%)	83.0 (61.5%)
$tZj$	170.0 (58.5%)	155.6 (67.2%)	148.7 (95.6%)	139.8 (63.7%)
$WZ$	164.3 (4.2%)	146.9 (89.4%)	138.2 (94.1%)	71.5 (51.7%)
Total	578.0 (12.3%)	457.2 (79.1%)	422.0 (92.3%)	294.3 (69.8%)
$M_{T'} \text{ (GeV)}$	$n_b \equiv 1$	cut (3.5)	cut (3.7)	cut (3.8)
800	25.5 (64.8%)	23.8 (93.6%)	22.2 (93.2%)	20.8 (93.6%)
1000	16.4 (63.2%)	15.4 (93.8%)	14.3 (92.4%)	13.4 (94.0%)
1200	10.1 (62.4%)	9.5 (94.2%)	8.7 (92.3%)	8.1 (92.3%)
1400	4.8 (60.1%)	4.5 (93.5%)	4.1 (92.1%)	3.8 (91.3%)
1600	2.2 (58.3%)	2.1 (93.3%)	1.9 (92.2%)	1.7 (90.0%)

Table 3: Object selection surviving events (and efficiencies with respect to the previous item). Signal computed for  $g^* = 0.1$  and  $R_L = 0.5$ .

Contrary to Ref. [12], we do not require a forward jet to not suppress any further the signal, despite it being a distinctive feature of our signature. This is also not necessary: the signal is already clearly visible above the background in the distribution of the transverse mass of the  $T'$  decay products (the 3 charged leptons and the  $b$ -jet), as can be seen in Fig. 2 for the various signal benchmark points.

We select a window around the peak of each benchmark point to get the best signal-over-background significance and we collect the final numbers in table 5.

### 3.2 Multivariate analysis

In section 3.1 we showed that suitable cuts on the most straightforward distributions were sufficient to isolate the signal from the background. We made use of the signal topology, which has a  $Z$  boson decaying leptonically, and a top-quark decaying into a  $b$ -jet and into a leptonic  $W$ -boson. The presence of the intermediate  $T'$  was then seen as a peak in the transverse mass of all its visible decay products. One could wonder if this was the best strategy, i.e. cutting on those variables with the values we chose. There are in fact many additional variables that one could analyse to distinguish the signal from the background. However, cutting on any of these variables will unavoidably reduce also the signal. To overcome this, several variables can be combined using a multivariate analysis (MVA) to obtain the best signal/background discrimination [36]. We identified some discriminating variables in table 4, ranked according to their discriminating power when a boosted decision tree (BDT) is employed. Here,  $\Delta\varphi$  is the difference of the azimuthal angles between 2 objects,  $\Delta\eta$  is the difference of their pseudorapidities, and  $\Delta R = \sqrt{(\Delta\varphi)^2 + (\Delta\eta)^2}$ .

To define some of the angular variables, the whole four-momentum of the neutrino stemming from the semileptonic top-quark decay has been reconstructed as described above. Furthermore, we did not include the top mass (neither as invariant mass nor as transverse mass of its decay products) in the MVA because it did not show a strong discriminating power. This is understandable because signal and the largest sources of



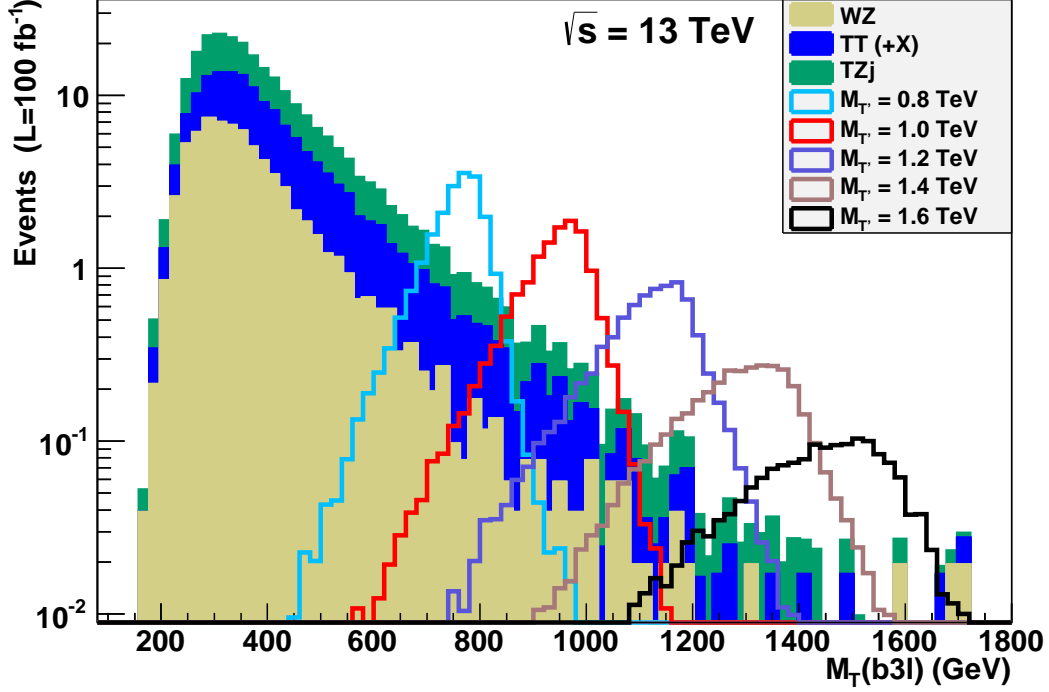


Figure 2: Transverse mass distribution for the  $T'$  decay products: the 3 charged leptons and the  $b$ -jet.

Variable	Importance	Variable	Importance
$M_T(b3\ell)$	$2.60 \cdot 10^{-1}$	$\Delta R(b, \ell_W)$	$9.77 \cdot 10^{-2}$
$p_T(Z)/M_T(b3\ell)$	$9.41 \cdot 10^{-2}$	$\Delta\varphi(t, Z)$	$8.17 \cdot 10^{-2}$
$\eta^{max}(j)$	$6.02 \cdot 10^{-2}$	$\Delta\varphi(\ell\ell _Z)$	$5.89 \cdot 10^{-2}$
$\Delta\varphi(Z, \not{p}_T)$	$5.37 \cdot 10^{-2}$	$p_T(j_1)/M_T(b3\ell)$	$5.08 \cdot 10^{-2}$
$\Delta\eta(\ell\ell _Z)$	$5.05 \cdot 10^{-2}$	$\Delta\eta(b, \ell_W)$	$5.03 \cdot 10^{-2}$
$\eta(t)$	$4.99 \cdot 10^{-2}$	$\Delta\varphi(Z, \ell_W)$	$4.63 \cdot 10^{-2}$
$\eta(Z)$	$4.61 \cdot 10^{-2}$		

Table 4: Ranking training variables for  $M_{T'} = 1.0$  TeV and full background. Here  $\ell\ell|_Z$  identifies the 2 leptons that reconstruct the  $Z$  boson.

background both have a top quark in their intermediate states. Finally, the presence of a forward jet is a prominent feature of the signal. To account for this, we use the largest pseudorapidity of all jets  $\eta^{max}(j)$  in the event.

It is interesting to notice that there are few variables which behaviour is directly proportional to the  $T'$  mass, like the  $p_T$  of the leading jet or the  $p_T$  of the 2 leptons reconstructing the  $Z$  boson. These correlations are efficiently removed if one consider ratios of the  $p_T$ 's over  $M_T(b3\ell)$ , which in fact decorrelate them. We checked that the

highest sensitivity is reached when the ratio of said variables to the  $T'$  reconstructed mass ( $M_T(b3\ell)$ ) is considered instead of the actual observables. All other variables are almost uncorrelated, with a degree of correlation of  $\pm 30\%$  at most.

The variables in table 4 are used to train the BDT to recognise the signal against the background. They are selected after the  $Z$  mass reconstruction, i.e. after applying eq. (3.5). A pictorial representation of these variables is in the Appendix, for the  $M_{T'} = 1.0$  TeV with  $R_L = 0.5$  benchmark point, and for the sum of all backgrounds. The BDT trained on each benchmark point is then applied on the full signal and background samples. A cut is then performed on the BDT output to get the best signal-over-background significance. Values of the cuts and best significances are collected in table 5.

We conclude this section with some further comments. Firstly, we checked that the MVA does not suffer for overtraining as follows. Each sample (signal and background) is divided into 2 independent subsamples, one that is used for training and the other one for comparison. The absence of overtraining issues is shown in Fig. 9: the output for the 2 subsamples coincides.

Secondly, we trained the MVA on the benchmark points (for  $g^* = 0.1$  and  $R_L = 0.5$ ). In section 3.3 we will make use of eq. (2.4) to extend the MVA analysis onto the whole  $g^*-R_L$  plane, without the need to retrain the BDT any further. However, by controlling the share of the  $T'$  coupling between first and third generation quarks,  $R_L$  changes the ratio of incoming sea/valence quarks, which ultimately alters the process kinematics. We directly checked that the loss in performance, as compared to the results obtained with the suitable training, is at most of  $\mathcal{O}(10\%)$  when  $R_L$  goes to zero, thereby validating our extrapolation procedure<sup>3</sup>.

Finally, the reader could wonder if the ratio of variables as described above might let the training procedure be less  $M_{T'}$ -dependent. It is in fact the case, but still it is not possible to use a universal MVA training and apply it to all the various  $T'$  samples. This is because, as clear from table 4, still  $M_T(b3\ell)$  is by far the best discriminating variable. If we remove it from the training, this becomes less  $M_{T'}$ -dependent for large  $T'$  masses, but the overall performance of the MVA is even lower than previously. This let us conclude that it is not possible to create an efficient  $M_{T'}$ -independent training scheme.

### 3.3 Results

We collect here the final results for the discovery power at the LHC. In the case of the cut-and-count analysis of section 3.1, we need to select a window around the signal peaks in the  $M_T(b3\ell)$  distribution. For the MVA of section 3.2, we need to perform a cut on the BDT output that maximises the significance. The maximum significance for the benchmark points, evaluated as  $\sigma = S/\sqrt{S+B}$  after selecting a window around the mass peak or cutting on the BDT output, are collected in table 5.

One of the most important result in this paper is that the dedicated BDT analysis does not significantly improve on the cut-and-count strategy, as clear from table 5. The latter analysis is certainly sufficient and easier. The cuts as displayed in eqs. (3.7)–(3.8)

---

<sup>3</sup>Notice that the typical precision that one can aim at with a fast simulation is  $\mathcal{O}(30\%)$ .

Analysis	$M_{T'} = 0.8$ TeV	$M_{T'} = 1.0$ TeV	$M_{T'} = 1.2$ TeV	$M_{T'} = 1.4$ TeV	$M_{T'} = 1.6$ TeV
$M_T(b3\ell)$ cut (GeV)	[800 – 860]	[840 – 1200]	[1000 – 1340]	[1120 – 1640]	[1200 – 1800]
S (ev.)	18.00	12.28	7.16	3.40	1.57
C&C B (ev.)	8.90	4.88	1.74	0.90	0.63
$\sigma$	3.47	2.96	2.40	1.64	1.06
MVA cut	0.07	0.08	0.11	0.12	0.12
$\sigma$	3.64	3.10	2.50	1.62	1.15

Table 5: Signal and background events and maximum significance for the benchmark points for  $\mathcal{L} = 100 \text{ fb}^{-1}$ , after selecting a mass window (for the C&C), or after cutting on the BDT output (MVA).

are already best optimised, as is the signal peak selection. No further variable/cut need to be considered/applied.

The significances in table 5 are for the benchmark points, evaluated for  $g^* = 0.1$  and  $R_L = 0.5$ . We can now extrapolate them to the full  $g^*-R_L$  parameter space using eq. (2.4). For simplicity, we applied it to the results of the MVA analysis of section 3.2, where a single cut is sufficient to evaluate the final significance. We cross checked for few parameter points that the extrapolation of the cut-and-count analysis of section 3.1 gives similar results. The 3 and 5 sigma discovery lines are drawn as a function of  $g^*$  and the  $T'$  mass for some fixed values of  $R_L$  in Fig. 3(left), and as a function of  $g^*$  and  $R_L$  for the benchmark  $T'$  masses in Fig. 3(right). Fig. 3 shows that with  $100 \text{ fb}^{-1}$  of data,  $T'$  masses up to 2 TeV can be observed, depending on the values of the couplings. The cross section for the trilepton decay channel of the  $T'$  (and hence the LHC reach) increases considerably when  $R_L$  is non-vanishing, getting to a maximum for  $R_L \simeq 1$ , corresponding to 50%–50% mixing.

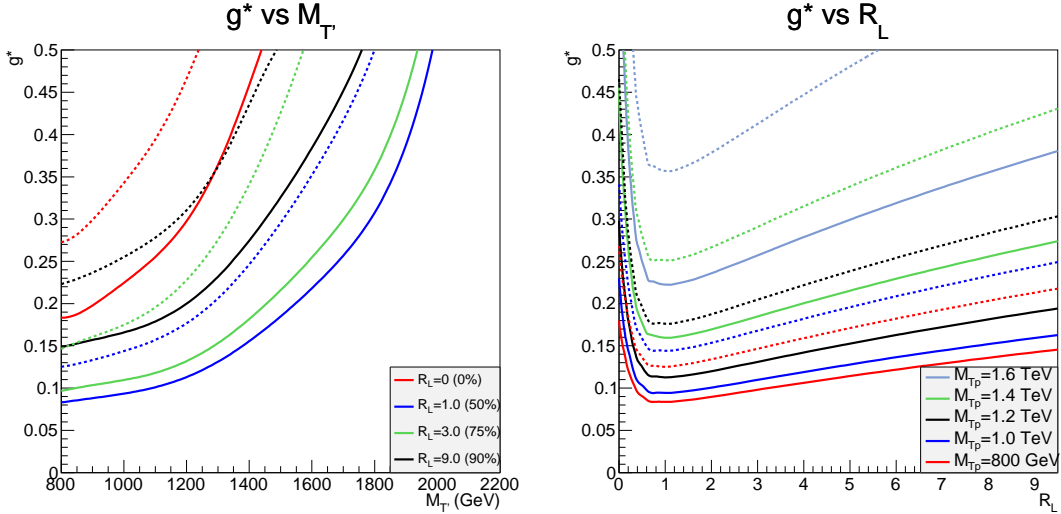


Figure 3: Significance  $\sigma = 3$  (solid lines) and  $\sigma = 5$  (dashed lines) for  $\mathcal{L} = 100 \text{ fb}^{-1}$ .

The reach in  $g^*$  is here roughly twice than for the no mixing case ( $R_L = 0$ ). Then, for larger values of  $R_L$ ,  $g^*$  needs to slightly increase to compensate for the decrease in

cross section due to the larger mixing with the first generation quarks, that suppress the  $T' \rightarrow tZ$  branching ratio.

The discovery power of the trilepton channel can be compared to the one of the dilepton channel as studied in [20]. The  $R_L = 0$  line in Fig. 3 is the one considered therein. However, to be able to draw a meaningful comparison, we shall set ourselves in the same conditions<sup>4</sup>, which correspond to the end of the LHC run-II. The plot for this setup is in Fig. 4. The curve to be compared is the  $R_L = 0$  one on the left-hand side plot. At low  $T'$  masses, the dileptonic channel of Ref. [20] performs slightly better, meaning that a marginally lower value of  $g^*$  can be probed. At larger  $T'$  masses though the trileptonic channel is more sensitive, extending the reach by 200 – 300 GeV. In these conditions, our analysis is sensitive to  $g^*$  couplings down to 0.05 and  $T'$  masses up to 2.1 TeV at most.

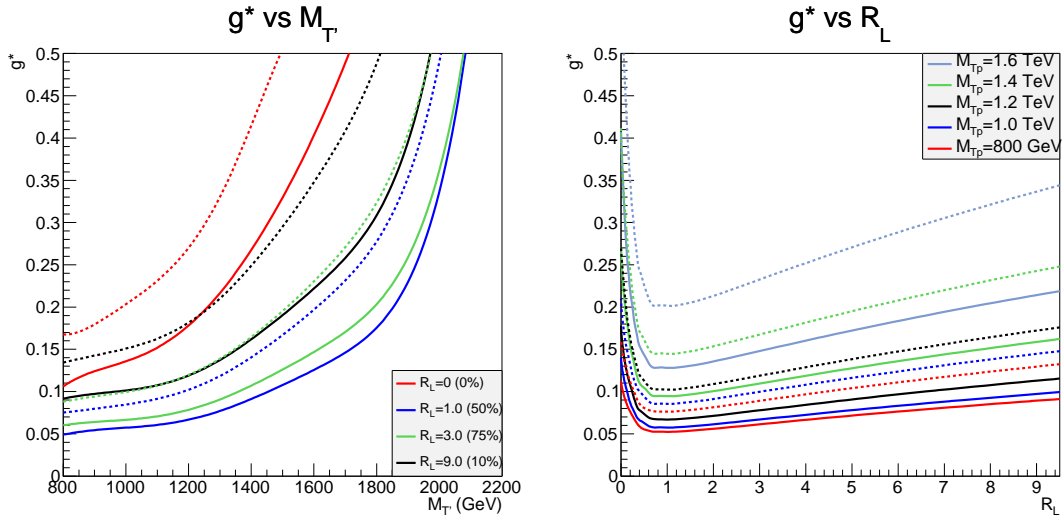


Figure 4: Significance  $\sigma = 3$  (solid lines) and  $\sigma = 5$  (dashed lines) for  $\mathcal{L} = 300 \text{ fb}^{-1}$  and  $k_f = 1.14$  as in Ref. [20].

### 3.4 Top FCNC reinterpretation

We conclude this paper by presenting a possible reinterpretation of our investigation in terms of the top-quark FCNC coupling to an up quark and a  $Z$  boson. In this scenario, the top quark interacts with a  $Z$  boson and a up- or charm-quark via the  $\kappa_{zqt}$  FCNC coupling [37]

$$\mathcal{L} = \frac{g}{\sqrt{2}c_W} \frac{\kappa_{zqt}}{\Lambda} \bar{t} \sigma^{\mu\nu} (f_{Zq}^L P_L + f_{Zq}^R P_R) q Z_{\mu\nu}. \quad (3.9)$$

In the following we restrict ourselves to the up-quark only. The operator in eq. (3.9) gives a similar final state as the one subject of this paper,  $pp \rightarrow tZ$ , with a top-quark and a  $Z$  boson produced back-to-back. The only difference with the  $T'$ -induced topology is the absence of the forward jet at leading order. The analyses of the  $T'$ -mediated signature subject of this paper could therefore be as well sensitive to the one induced by the top

<sup>4</sup>Ref. [20] used an integrated luminosity of  $300 \text{ fb}^{-1}$  and rescaled the signal by a mean  $k$ -factor of 1.14.

Cut	Events(eff.)
no cuts	2263(100%)
$1 \leq n_j \leq 3$	1765(78.9%)
$n_\ell \equiv 3$	191.8(10.9%)
$n_b \equiv 1$	113.8(59.3%)
cut (3.5)	103.2(90.7%)
cut (3.7)	96.2(93.3%)
cut (3.8)	91.1(94.7%)
$M_T(b3\ell) > 400 \text{ GeV}$	
S	68.0
B	102.9
$\sigma$	5.2

Table 6: Object selection surviving events (and efficiencies with respect to the previous item) for the cut-and-count analysis of the FCNC top coupling  $K_{tZu}$  and signal/background events that maximise the significance.

effective coupling. We tested it by producing a leading order  $pp \rightarrow tZ$  sample and by running it on the cut-and-count analysis of section 3.1. Efficiencies and event yields for  $100 \text{ fb}^{-1}$  are collected in table 6.

The  $M_T(b3\ell)$  distribution after the application of the cuts of eqs. (3.5)–(3.8) is shown in Fig. 5. The significance is maximised by selecting  $M_T(b3\ell) > 400 \text{ GeV}$ , reaching the value of 5.2 sigma for the present best limit of the coupling of  $\kappa_{zut} = 0.2 \text{ TeV}^{-1}$  [38]. For comparison, we applied the MVA trained on each  $T'$  signal to the FCNC case. Also in this case however it did not improve the sensitivity.

Finally, the cut-and-count discovery power curves at the LHC as a function of the top FCNC coupling for  $100 \text{ fb}^{-1}$  and  $300 \text{ fb}^{-1}$  are shown in figure 6. This analysis can gather evidences for the existence of FCNC processes in the top sector for couplings above 0.14(0.10) for 100(300)  $\text{fb}^{-1}$ . In case of non observation, 95% C.L. limits can be put for couplings down to 0.12 and 0.08 for the two integrated luminosities, respectively.

## 4. Conclusions

In this work we described the LHC run-II discovery potential of the trilepton channel for a singlet top partner in the single production mode and its subsequent decay into a top quark and a  $Z$  boson. A simple cut-and-count analysis has been designed, by selecting and cutting the most straightforward distributions. A suitable multivariate analysis did not improve significantly on the cut-and-count results. The comparison was performed on several signal benchmark points. Further, we proposed a simple way to extend our results to the whole parameter space of a simplified model. The extrapolation has been performed on the results of the MVA solely because simpler, and it has been cross checked that the cut-and-count analysis gives similar results.

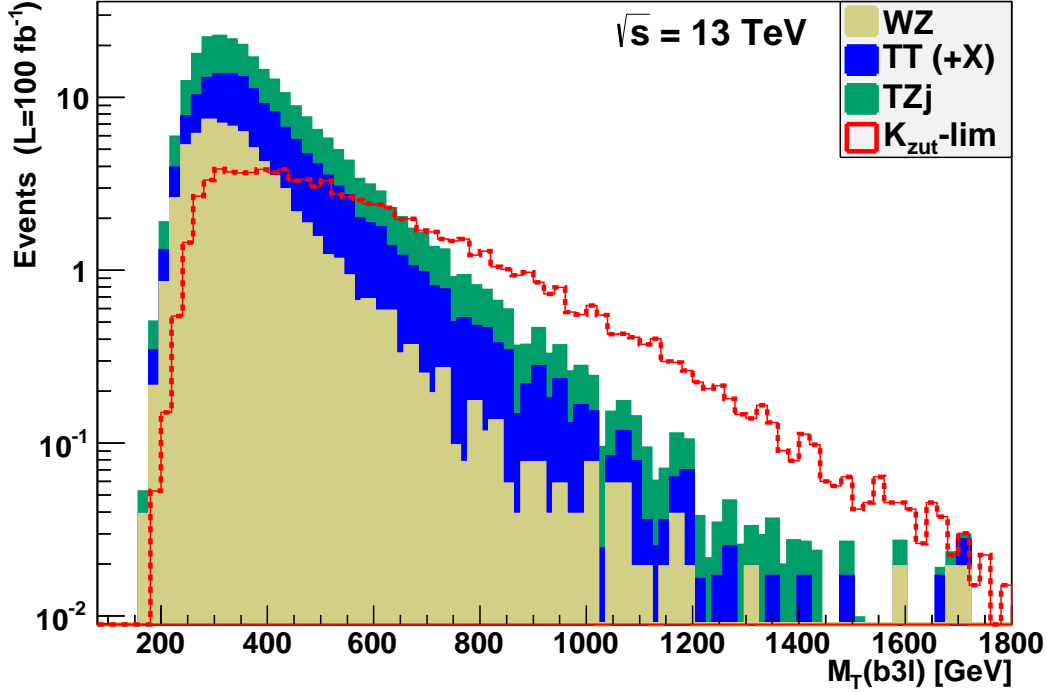


Figure 5:  $M_T(b3\ell)$  distribution with the present best limit on the top-Z-up FCNC coupling.

Overall, a search at the LHC in the trilepton channel can be sensitive to top partners decaying into  $tZ$  for masses up to 2.0(2.1) TeV and couplings down to 0.08(0.05) with 100(300)  $\text{fb}^{-1}$  of data. We compared to the reach in the dilepton channel of Ref. [20], concluding that the trilepton mode can extend the former by 200 – 300 GeV in  $T'$  masses for suitable values of the couplings. Finally, we reinterpreted our analyses in the context of a top FCNC coupling to a  $Z$  boson and an up quark, which provides a similar final state. We showed that this channel can discover at  $5\sigma$  values of the couplings at the present best exclusion limit (for 100  $\text{fb}^{-1}$ ), probe at  $3\sigma$  values down to 0.14(0.10) for 100(300)  $\text{fb}^{-1}$ , or eventually extend the exclusion limits down to 0.12 and 0.08 for the two integrated luminosities, respectively.

## Acknowledgements

We would like to sincerely thank our colleagues A. Alloul, C. Collard, E. Conte and G. Hamad and for the help in generating the background samples used in this work and for useful comments. The work of LB is supported by the Theorie-LHC France initiative of the CNRS/IN2P3 and by the French ANR 12 JS05 002 01 BATS@LHC.

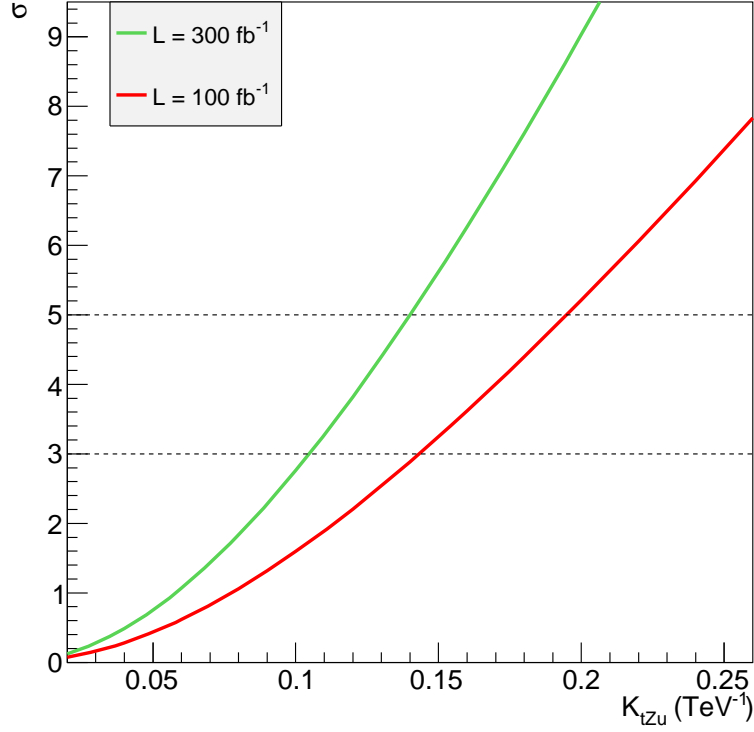


Figure 6: Significance as a function of the top FCNC coupling for the cut-and-count analysis.

## Appendix: BDT variables

We present here the training variables for the  $M_{T'} = 1.0$  TeV with  $R_L = 0.5$  benchmark point. The overtraining test, shown in figure 9, shows that there is no overtraining issue.

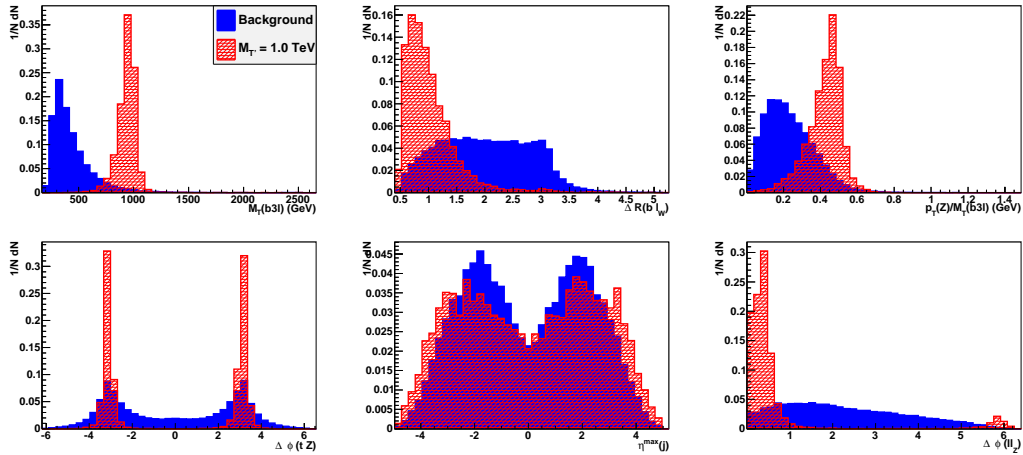


Figure 7: BDT training variables (1).

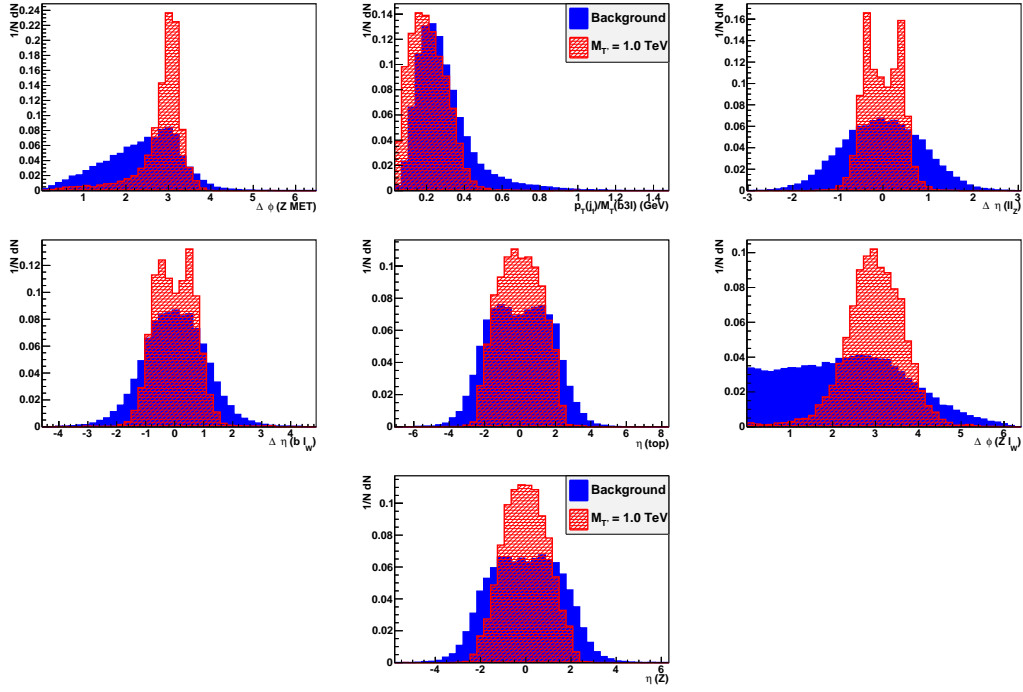


Figure 8: BDT training variables (2).

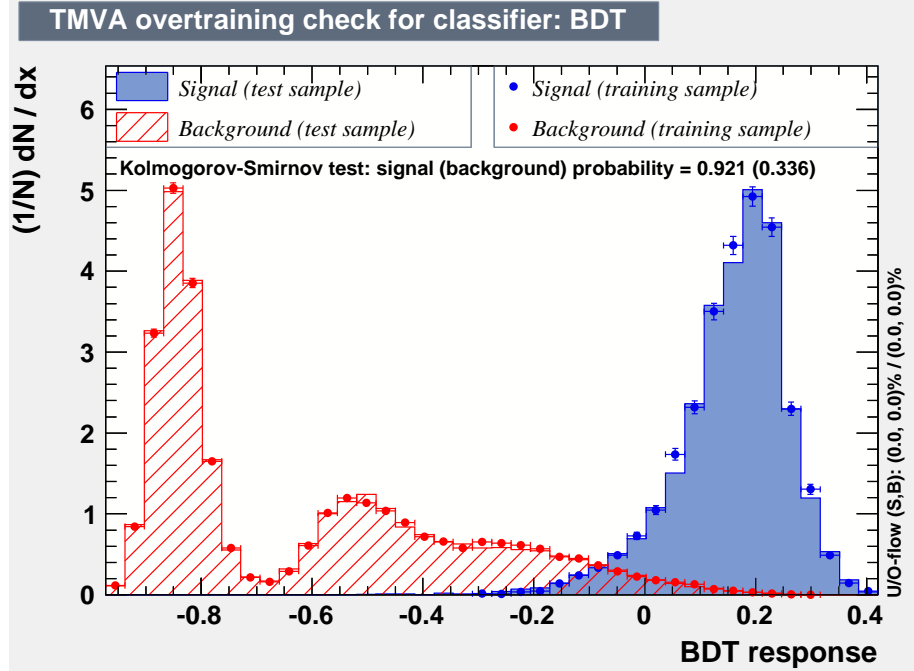


Figure 9: BDT overtraining.



## References

- [1] CMS Collaboration, S. Chatrchyan et al., Phys.Lett. **B716**, 30 (2012), arXiv:1207.7235.
- [2] ATLAS Collaboration, G. Aad et al., Phys.Lett. **B716**, 1 (2012), arXiv:1207.7214.
- [3] R. Contino, L. Da Rold, and A. Pomarol, Phys.Rev. **D75**, 055014 (2007), arXiv:hep-ph/0612048.
- [4] R. Contino, T. Kramer, M. Son, and R. Sundrum, JHEP **0705**, 074 (2007), arXiv:hep-ph/0612180.
- [5] R. Contino and G. Servant, JHEP **0806**, 026 (2008), arXiv:0801.1679.
- [6] C. Anastasiou, E. Furlan, and J. Santiago, Phys.Rev. **D79**, 075003 (2009), arXiv:0901.2117.
- [7] N. Vignaroli, Phys.Rev. **D86**, 075017 (2012), arXiv:1207.0830.
- [8] O. Matsedonskyi, G. Panico, and A. Wulzer, JHEP **1301**, 164 (2013), arXiv:1204.6333.
- [9] S. A. Ellis, R. M. Godbole, S. Gopalakrishna, and J. D. Wells, JHEP **1409**, 130 (2014), arXiv:1404.4398.
- [10] F. del Aguila, M. Perez-Victoria, and J. Santiago, JHEP **0009**, 011 (2000), arXiv:hep-ph/0007316.
- [11] ATLAS Collaboration, G. Aad et al., (2014), arXiv:1409.5500.
- [12] CMS Collaboration, S. Chatrchyan et al., Phys.Lett. **B729**, 149 (2014), arXiv:1311.7667.
- [13] J. Berger, J. Hubisz, and M. Perelstein, JHEP **1207**, 016 (2012), arXiv:1205.0013.
- [14] A. De Simone, O. Matsedonskyi, R. Rattazzi, and A. Wulzer, JHEP **1304**, 004 (2013), arXiv:1211.5663.
- [15] J. Aguilar-Saavedra, EPJ Web Conf. **60**, 16012 (2013), arXiv:1306.4432.
- [16] J. Aguilar-Saavedra, R. Benbrik, S. Heinemeyer, and M. Perez-Victoria, Phys.Rev. **D88**, 094010 (2013), arXiv:1306.0572.
- [17] G. Cacciapaglia et al., JHEP **1203**, 070 (2012), arXiv:1108.6329.
- [18] M. Buchkremer, G. Cacciapaglia, A. Deandrea, and L. Panizzi, Nucl.Phys. **B876**, 376 (2013), arXiv:1305.4172.
- [19] G. Brooijmans et al., (2014), arXiv:1405.1617.
- [20] J. Reuter and M. Tonini, (2014), arXiv:1409.6962.
- [21] J. Pumplin et al., JHEP **0207**, 012 (2002), arXiv:hep-ph/0201195.
- [22] J. Alwall et al., JHEP **1407**, 079 (2014), arXiv:1405.0301.
- [23] T. Sjostrand, S. Mrenna, and P. Z. Skands, JHEP **0605**, 026 (2006), arXiv:hep-ph/0603175.
- [24] R. Field, Acta Phys.Polon. **B42**, 2631 (2011), arXiv:1110.5530.
- [25] DELPHES 3, J. de Favereau et al., JHEP **1402**, 057 (2014), arXiv:1307.6346.
- [26] M. Cacciari, G. P. Salam, and G. Soyez, Eur.Phys.J. **C72**, 1896 (2012), arXiv:1111.6097.
- [27] M. Cacciari, G. P. Salam, and G. Soyez, JHEP **0804**, 063 (2008), arXiv:0802.1189.

- [28] A. Alloul, N. D. Christensen, C. Degrande, C. Duhr, and B. Fuks, *Comput.Phys.Commun.* **185**, 2250 (2014), arXiv:1310.1921.
- [29] [http://feynrules.irmp.ucl.ac.be/wiki/VLQ\\_tsingletvl](http://feynrules.irmp.ucl.ac.be/wiki/VLQ_tsingletvl).
- [30] M. Czakon, P. Fiedler, and A. Mitov, *Phys.Rev.Lett.* **110**, 252004 (2013), arXiv:1303.6254.
- [31] CMS Collaboration, V. Khachatryan et al., *Eur.Phys.J.* **C74**, 3060 (2014), arXiv:1406.7830.
- [32] E. Conte, B. Fuks, and G. Serret, *Comput.Phys.Commun.* **184**, 222 (2013), arXiv:1206.1599.
- [33] E. Conte, B. Dumont, B. Fuks, and C. Wymant, *Eur.Phys.J.* **C74**, 3103 (2014), arXiv:1405.3982.
- [34] CMS Collaboration, S. Chatrchyan et al., *JINST* **8**, P04013 (2013), arXiv:1211.4462.
- [35] V. D. Barger, T. Han, and R. Phillips, *Phys.Rev.* **D36**, 295 (1987).
- [36] A. Hoecker et al., *PoS ACAT*, 040 (2007), arXiv:physics/0703039.
- [37] J. Aguilar-Saavedra, *Nucl.Phys.* **B812**, 181 (2009), arXiv:0811.3842.
- [38] CMS Collaboration, S. Chatrchyan et al., *Phys.Rev.Lett.* **112**, 171802 (2014), arXiv:1312.4194.